Multichannel Active Sound Quality Control for Independent-Channel Sound Profiling

Jaime A. Mosquera-Sánchez, Wim Desmet
Department of Mechanical Engineering, KU Leuven, Celestijnenlaan 300, 3001 Heverlee, Belgium

Karl Janssens
Siemens Industry Software NV, Interleuvenlaan 68, Belgium

Leopoldo P. R. de Oliveira
São Carlos School of Engineering, University of São Paulo, Av. Trabalhador Sancarlense 400, São Carlos 13566-590, Brazil

Summary
Multichannel active noise control algorithms have been proposed to deal with sound propagation in enclosures, which base their operation on sensor/actuator positioning conditions that in some applications could not be easily met. In this paper, we investigate a multichannel active sound quality control algorithm, intended to independently control each sensor position, regardless of the acoustic coupling among channels. The decentralized channels share their adaptive weights among each other, in order to extract the maximum allowed gain that minimizes the cost function at the corresponding error sensor, while keeping distortion at the other error sensors as low as possible. A coupled FE-FE vibro-acoustic model of a scaled vehicle mock-up is used for computer simulations, which properly reproduces acoustic coupling among the error sensors. A pure-sinusoid disturbance is used as the input to the vibroacoustic model, and a 2x2 multichannel algorithm is proposed to independently profile it. Computer simulations demonstrate that, despite of the increased computational burden, as compared with the decentralized leaky-LMS control algorithm, the proposed algorithm is able to deal with the acoustic coupling among the error sensors, thus reaching independent control targets over the disturbance in each error sensor, regardless of their position in an enclosure.

PACS no. 43.50.Ki

1. Introduction

When disturbances propagate into enclosures, it is often desired to implement control actions at several positions. Unlike the conventional multichannel Active Noise Control (ANC) framework, multichannel Active Sound Quality Control (ASQC) systems are not mainly concerned with obtaining the same auditory condition at all error sensor positions. To this regard, decentralization of multichannel control systems seems to be a suitable strategy for attaining independent auditory perceptions per channel, once that each control module is only concerned with its corresponding set of error sensors. However, since acoustic coupling among channels is commonly encountered in enclosures, the control actions performed for a given set of error sensors can undesirably amplify, reduce, or even shift the relative phase of the primary disturbance at other positions, which for the derivations worked out in this paper, is composed of K pure-sinusoid signals, as follows:

$$d[n] = \sum_{k=1}^{K} a_k e^{-j(\omega_k n + \phi_k)}, \tag{1}$$

with d being the primary disturbance; $\{a,\ \omega,\ \phi\}$ are the amplitude, frequency ($\omega = 2\pi f$), and relative phase of the k^{th} narrowband component, respectively, and n is a time-domain index, related to the system's sampling rate Fs.

Some efforts have been made to face the interaction among decentralized control modules in multichannel arrays, either by means of optimum Sensor-Actuator Pair (SAP) positioning [1, 3, 5], or by constraining the controller effort [6, 7]. While some applications allow positioning of sensors and/or actuators with some degree of freedom, imposition of output constraints is often the preferred solution in situations where such a design parameter is restricted, which in turn brings the benefit of extending the actuators' lifecycle, at the expense of degrading the controller performance.

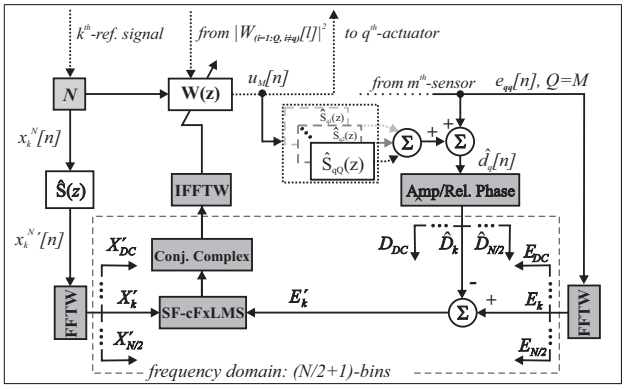

Figure 1. Block diagram of the k^{th} control module of the multichannel ASQC algorithm.

In this paper, we are concerned with the second type of problems, where low distortion levels at other than the m^{th} error sensor position are required, by means of constraining the filter gain of the channels of the control array. We introduce a decentralized ASQC algorithm, whose q^{th} control unit compares its adaptive filter gain at the k^{th} frequency to the other $Q-1$ ones in the system, to determine to what extend it can be increased, without causing distortion. This constraint is formulated as a set of exterior penalty functions [9, 10], and we hereby briefly discuss the equivalence of this formulation, to that of constraining the q^{th} adaptive filter gain to the ∞-norm of the other controllers. Section 2 derives the algorithm, Section 3 discusses computer simulations of the algorithm, and Section 4 is devoted to present some final remarks.

2. Multichannel ASQC Algorithm

From Figure 1 that illustrates the q^{th} control module, the frequency-domain pseudo-error signal $E' \in \mathbb{C}^{(N/2+1)}$ is obtained, as follows:

$$E'_{qq}[l] = E_q[l] - \widehat{D}_q[l] = W_q[l]X'^N_{qj}[l], \qquad (2)$$

where $l = t(LT_s)$; $t = 1,\ 2,\ \ldots$, is a time-domain variable that indexes the data block operations, with L being the length of the time-domain buffers required to perform the internal N-point FFT operations, $L = N$, and $T_s = 1/F_s$ is the sample rate of the system; $\left\{E,\ \widehat{D},\ X,\ W\right\} \in \mathbb{C}^{(N/2+1)}$ are the frequency-domain representations of the error, estimated primary disturbance, reference signal and adaptive filter, respectively; the superscript $(')$ denotes application of the secondary path $\widehat{S}_{qj}(z)$, from the j^{th} actuator to the q^{th} error sensor, over X^N; and the superscript N stands for normalization of $x[n]$ by using the NEX-LMS strategy [4].

Previous work [8] has demonstrated that the frequency-domain updating algorithm can be enhanced to deal with combinations of periodic and impulsive disturbances, by weighting the most recent incoming data, instead of estimating the gradient of the cost function by using the entire time history of the involved signals. Therefore, the cost function is stated as follows:

$$J_q[l] = \sum_{\tau=0}^{l} \rho_q^{(l-\tau)} \left(E'_{qq}[\tau]E'^*_{qq}[\tau]\right), \qquad (3)$$
$$\text{s. t.}\,\{max\,[0,\ c_j\,(W_q[l])]\}^2;\ j = 1,\ldots\ Q;\ j \neq q,$$

where $\tau \in \mathbb{Z}^+$ is a time-domain index, related to l; $\rho \in [0,\ 1)$ is a forgetting factor; and the second line of Eq. 3 describes a set of $Q-1$ constraints over the q^{th} control module, where $c(W)$ is a mathematical operator that will be defined next.

The constraint in Eq. 3 consists of the continuous inspection of the other $Q-1$ filter gains at the k^{th} frequency, in order not to allow the q^{th} controller to converge to higher than the other gains. This constraint can be written as follows:

$$|W_q[l]|^2 < |W_j[l]|^2, \qquad (4)$$
$$c_j\,(W_q[l]) = |W_q[l]|^2 - |W_j[l]|^2 < 0$$

which is a quadratic expression in W_q. The fact that the constraint be squared in Eq. 3 makes $\Phi_q[l]$ (Eq. 5) to have continuous first derivative [10].

From adaptive control theory, it is known that as $\{n,\ l\} \to \infty$, the decentralized adaptive filter $W_q \to P_q(z)/S_{qq}(z)$, i.e, the q^{th} adaptive filter converges to the primary path dynamics, while inversely represents the secondary path dynamics. Unlike the development carried out by Rafaely and Elliott [9] for the single-channel case, where the filter gain is constrained to its own ∞-norm, the condition in Eq. 3 shows that the q^{th} filter gain is restricted to the ∞-norm of the other adaptive channels, *at the k^{th} frequency*, i.e. to $\|P_q(\omega = k)/S_{qq}(\omega = k)\|_\infty$

A new cost function can therefore be stated, by using a penalty term $\sigma \in \mathbb{R}^+$, as follows:

$$\Phi_q[l] = \sum_{\tau=0}^{l} \rho_q^{(l-\tau)} \left(E'_{qq}[\tau]E'^*_{qq}[\tau]\right)$$
$$+ \sigma_q \sum_{\substack{j=1 \\ j\neq q}}^{Q} \{max\,[0,\ c_j\,(W_q[l])]\}^2 \qquad (5)$$

Since all the mathematical entities involved in the cost function in Eq. 5 are in the frequency domain, a complex-domain algorithm is needed to update the adaptive filter:

$$W_q[l+1] = W_q[l] - \mu_q\,[\text{Re}\,(\nabla\Phi_q[l])$$
$$+ \jmath\,\text{Im}\,(\nabla\Phi_q[l])], \qquad (6)$$

where $\jmath \in \mathbb{C} = \sqrt{-1}$, and $\{\text{Re},\ \text{Im}\}$ denotes real and imaginary part of a complex number.

While derivation of $\nabla_{(\mathrm{Re,Im})} J_q[l]$ for the first line of Eq. 5 has already been worked out by Mosquera-Sánchez and de Oliveira [8] for the single-channel control case, derivation of the set of penalty functions is done in a similar way as in Rafaely and Elliott [9], as follows:

$$\frac{\partial}{\partial W_q}\left\{max\left[0,\ c_j\left(W_q[l]\right)\right]\right\}^2 = \quad (7)$$

$$\begin{cases} 2\left[c_j\left(W_q[l]\right)\right]\dfrac{\partial}{\partial W_q} c_j\left(W_q[l]\right), & c_j\left(W_q[l]\right) > 0 \\ 0, & c_j\left(W_q[l]\right) \leq 0 \end{cases}$$

In Eq. 6 the piecewise function can be computationally implemented by using the following operator [9]:

$$[c_j(W_q[l])] = c_j(W_q[l])\frac{sign\left[c_j(W_q[l])\right]+1}{2} \quad (8)$$

where $sign()$ is the sign function, and $c_j(W_q[l])$ is as defined in Eq. 4. In Eq. 7 it is also required to calculate the derivative of $c_j\left(W_q[l]\right)$ with respect to $W_q[l]$. From Eq. 4 we see that $|W_j[l]|^2$ is constant with respect to $W_q[l]$, then we are concerned with $|W_q[l]|^2$, and therefore:

$$\frac{\partial\left|W_q[l]\right|^2}{\partial W_q} = \frac{\partial W_q[l]W_q^*[l]}{\partial Re(W_q)} + \jmath\frac{\partial W_q[l]W_q^*[l]}{\partial Im(W_q)} \quad (9)$$

The Discrete Fourier Transform (DFT) operation on the q^{th} adaptive filter is formulated as follows [9]:

$$W_{(q,k)}[l] = \sum_{n=0}^{N-1} w_n e^{-j2\pi nk/N} = W_q[l]a_k, \quad (10)$$

where a_k is a column vector of the complex Fourier weights at the k^{th} frequency. By substituting Eq. 10 in Eq. 9, it follows that:

$$\begin{aligned}\frac{\partial\left|W_q[l]\right|^2}{\partial W_q} &= W_q[l]a_k^* + W_q^*[l]a_k \\ &\quad + \jmath\left[-\jmath W_q[l]a_k^* + \jmath W_q^*[l]a_k\right] \\ &= 2W_q[l]a_k^*\end{aligned} \quad (11)$$

The iterative algorithm for the q^{th} control module in Eq. 6 is then obtained by using a previous result (cf. [7, 8]) and Eq. 11, as follows:

$$\begin{aligned}W_q[l+1] = W_q[l] + 2\mu_q\{&\gamma_{qq}[l] \\ &-2\sigma_q\sum_{\substack{i=1\\ i\neq q}}^{Q}\left[|W_q[l]|^2 - |W_i[l]|^2\right]W_q[l]a_k^*\Bigg\}\end{aligned} \quad (12)$$

where

$$\gamma_{qq} = \sum_{\tau=0}^{l}\rho_q^{(l-\tau)}\left[E'_{(qq)}[\tau]X'^{*N}_{(qq)}[\tau]\right] \quad (13)$$

Equation 13 with $\tau > 1$ is computationally demanding, however, the algorithm can be simplified by making $\tau = 1$, thus obtaining:

$$\gamma_{qq} = \rho_q\left[E'_{(qq)}[l]X'^{*N}_{(qq)}[l]\right], \quad (14)$$

which completes the proposed updating rule for the q^{th} control unit.

3. Computer Simulations

Computer simulations under *Simulink* v. 8.0 (*MATLAB* R2012b) have been run to demonstrate the operation of the proposed multichannel ASQC algorithm. The objective of the simulations is to control the disturbance at one position, while avoiding distortion at other targeted position. To do that, three $(1\times 2\times 2)$ (one reference signal, two outputs/inputs) multichannel frequency-domain algorithms are compared to each other: (i) SF-cFxLMS; (ii) SF-cFxLMS with constraint on the adaptive filter power (δ-SF-cFxLMS) [7]:

$$\begin{aligned}W_q[l+1] &= \Psi_q W_q[l] + 2\mu_q\gamma_{qq}[l] \\ \gamma_{qq}[l] &= \rho_k\gamma_k[l-1] + E'_{qq}[l]X'^{*N}_{qq}[l],\end{aligned} \quad (15)$$

where $\Psi_q = 1-\mu_q\delta_k$ is the constraint factor, also known as the *leak* parameter, which constraints its adaptive filter without considering other channels in the system; and (iii) the proposed algorithm. Whereas comparison between algorithms (ii) and (iii) shows two methods of constraining the adaptive filter gain, inclusion of algorithm (i) illustrates the effect of purposelessly amplifying/reducing, and/or shifting the relative phase of a narrowband component in $d[n]$.

The primary disturbance consists of a $160[Hz]$ pure-sinusoid signal. The sampling rate of the algorithms is $F_s = 2048[Hz]$. The algorithms have been implemented with internal buffers/FFTWs of $L = N = 64$ points, which makes $d[n]$ to exactly lie into the 5^{th} Fourier bin $(\#bin = (f_{(d[n])}N)/Fs)$. The controller parameters are then set up as: $\mu_{(5,1)} = 1.0e^{-02}$; $\rho_{(5,1)} = 5.0e^{-01}$; $\delta_{(5,1)} = 1e^{02}$; $\sigma_{(5,1)} = 7.5e^{06}$, respectively, which are the largest found values that still allow the algorithms to stably run, while attaining the fastest convergence. The simulations have also been contaminated with uncorrelated white noise at both error sensors, with variance equals to $1e^{-09}$.

In this paper we adopted a metric to quantify the *amount of distortion* caused at the 2nd position:

$$AD_i = \frac{\sum_{n=1}^{T}(e_i[n])^2}{\sum_{n=1}^{T}(d_i[n])^2}, \quad (16)$$

which should equal one when zero distortion is caused at the i^{th} position. $AD_i \to 0$ as $d[n] \to 0$, whereas $AD_i \to \infty$ as $d[n] \to \infty$. Table I summarizes the amounts of distortion obtained from simulations.

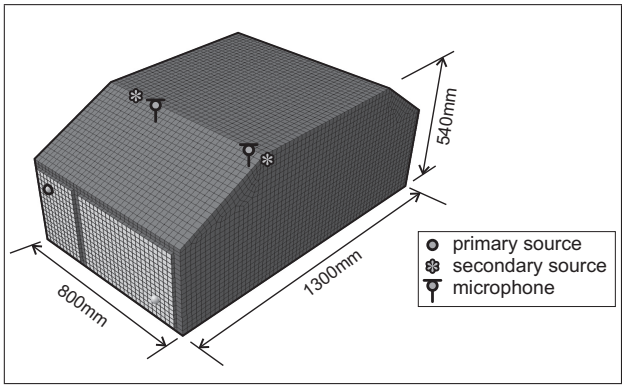

Figure 2. Coupled FE-FE model of a vehicle mock-up [2].

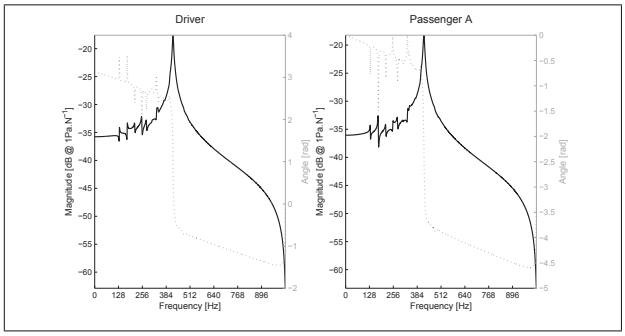

Figure 3. Primary paths dynamics.

3.1. Transfer Paths

Primary and secondary transfer paths are obtained from a coupled FE/FE model of a scaled simplified car geometry, which is shown in Figure 2. An Eulerian vibro-acoustic formulation is adopted, and the investigated bandwidth is $0-500[Hz]$. The structural mesh of the clamped steel firewall has 3712 degrees of freedom (DoF), as a result of using 512 4-noded shell elements. The acoustic mesh has 69272 DoFs, which is the result of using 8-noded brick elements. More details of the model and FE/FE formulation can be verified in de Oliveira et al. [2]. Sensor/actuator dynamics have been assumed as ideal.

Figure 3 shows the primary path dynamics from the structural input at the firewall to the error sensors placed close to driver and passenger heads. Figure 4 shows the control loops dynamics from the loudspeakers to the error sensors. Each actuator has been placed close to its corresponding error sensor, as suggested by Elliott and Boucher [5]. Discrete frequencies at which a multichannel active sound control can be decentralized have also been calculated by using a sufficient condition for SAP placement [5]. In Figure 4 these frequencies are highlighted with red points.

3.2. Results

3.2.1. Amplitude control

Figure 5 illustrates the effect of reducing the amplitude of the primary disturbance at the driver's position. Unconstrained reduction causes an amplification of the disturbance at the passenger's position (*cf.* Table I). Nevertheless, distortion is notoriously mitigated by implementing restrictions to the filter gain. The δ-constraint is more effective in limiting the output of the controller, hence attaining a better mitigation of the distortion at the passenger's position. By contraposition, the σ-constraint assesses the filter gain of the other controllers in the system, which could result in a less stringent constraint, thus causing more distortion at the other position. However, Table I re-

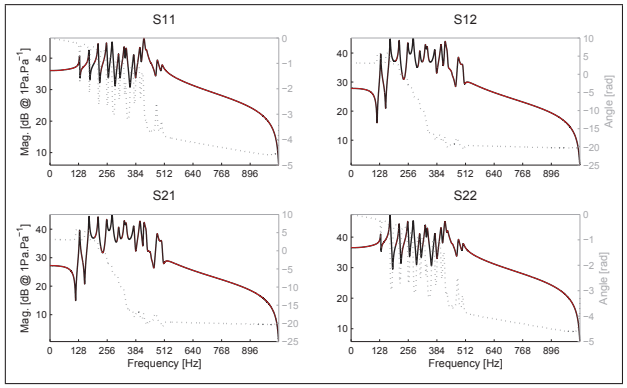

Figure 4. Secondary paths dynamics - Red points highlight *decentralized* frequencies.

Table I. Amount of distortions (adimensional)

Parameter	Algorithm	Pos. 01	Pos. 02
Amp.	No Constraint	0.0186	1.1907
	δ-Constraint	0.8260	1.0172
	σ-Constraint	0.6533	1.0363
Amp. + Impulses	No Constraint	0.2872	1.1436
	δ-Constraint	0.7795	1.0234
	σ-Constraint	0.6983	1.0334
Pha. No Constr.	$\angle d[n] = \pi/4$	1.0868	1.0799
	$\angle d[n] = \pi/2$	1.2615	1.2434
	$\angle d[n] = 3\pi/4$	1.4508	1.4201
	$\angle d[n] = \pi$	1.4791	1.4492
Pha. δ-Constr.	$\angle d[n] = \pi/4$	0.9529	1.0084
	$\angle d[n] = \pi/2$	0.8359	1.0222
	$\angle d[n] = 3\pi/4$	0.7156	1.0333
	$\angle d[n] = \pi$	0.6657	1.0349
Pha. σ-Constr.	$\angle d[n] = \pi/4$	0.9056	1.0207
	$\angle d[n] = \pi/2$	0.7440	1.0377
	$\angle d[n] = 3\pi/4$	0.6128	1.0480
	$\angle d[n] = \pi$	0.5637	1.0477

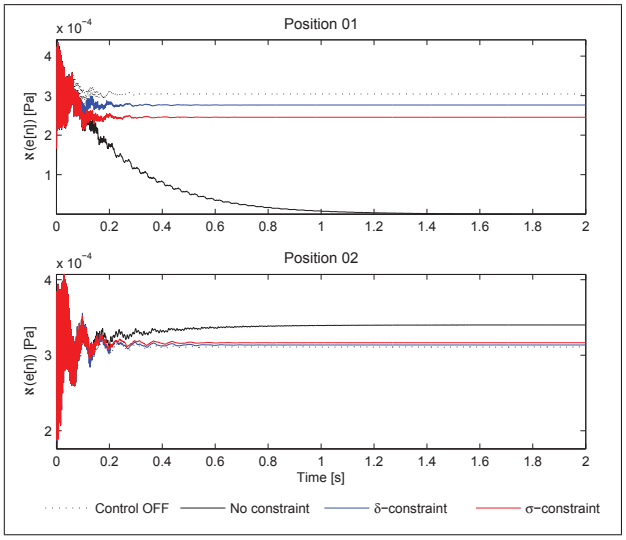

Figure 5. Control of the amplitude of $d[n]$.

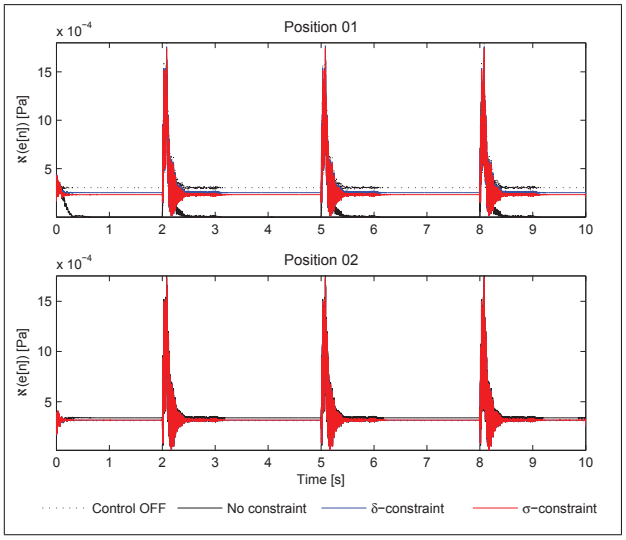

Figure 6. Control of the amplitude of $d[n]$ with impulsive disturbances.

veals that the difference between the two strategies is very small, regarding amount of distortion.

3.2.2. Impulsive occurrences

In this control situation, impulsive occurrences arising once each three seconds contaminate $d[n]$. The controller is then equipped with a forgetting factor $\rho = 5.0e^{-01}$ to improve its response. Figure 6 shows that, since the primary disturbance is quite simple, the algorithm further improved its initial convergence rate, going from $1[s]$ to $0.25[s]$. Two observations can be derived from Figure 6: (i) the forgetting factor improves the overall response of the algorithm; and (ii) both effort constraint strategies are compatible with this controller parameter. The δ-constraint strategy is again more effective than the σ one, due to the reasons already discussed.

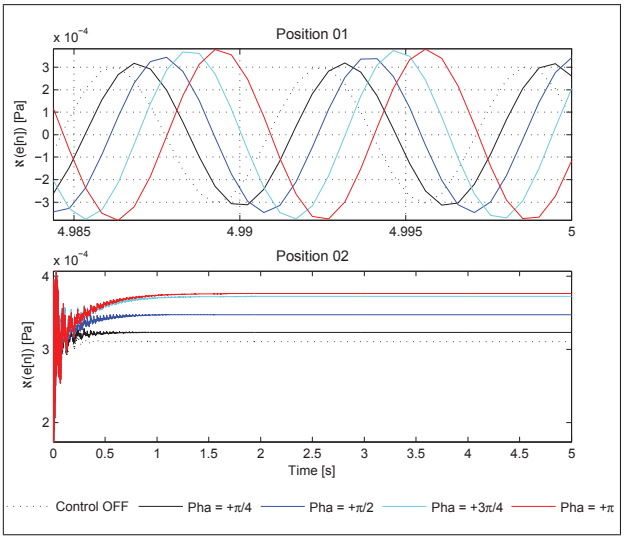

Figure 7. Control of the relative phase of $d[n]$ - no controller effort.

3.2.3. Relative-phase control

Control of the relative phase is shown to be an attractive means of positively modify psychoacoustic roughness of periodic disturbances, without performing corrections on the amplitude function [8]. The main issue when controlling such a parameter is the large controller effort required. Figure 7 shows some relative-phase shifts of $d[n]$ (from its original relative-phase value to $+\pi[rad]$), where it can be evidenced that these control actions do involve large amounts of distortion at the passenger's position. The situation is still worst, due to an undesired amplification at the same driver's position, as its relative-phase is shifted.

Figure 8 shows the implementation of the δ-constraint to the relative-phase control actions, whereas Figure 9 illustrates the effect of the σ one over the same relative-phase control actions. Although the figures reveal no significant differences, the δ constraint is once again more effective than the σ one. Moreover, the latter strategy exhibits oscillations during the convergence period, which is mainly due to the fact that the position one's control module reads the adaptive filter of the other one, when it is still converging. Even so, the overall system manages to stably converge to the steady-state.

4. Conclusion

In this paper, a multichannel active sound quality control algorithm for independent-channel sound profiling is introduced, which minimizes the error at a certain error sensor location, while keeping distortion at the other channels as low as possible. The cost function of the single-channel SF-cFxLMS algorithm is constrained to the ∞-norm of the other $Q-1$ channels in the decentralized multichannel system, at a given frequency. This strategy of constraining the filter gain

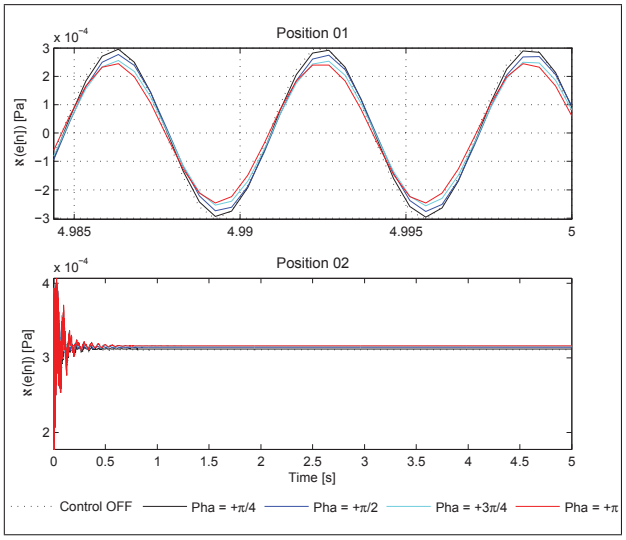

Figure 8. Control of the relative phase of $d[n]$ - δ-constraint.

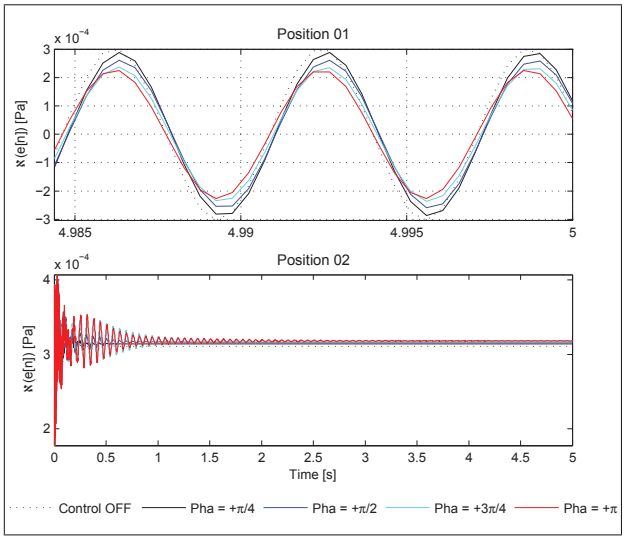

Figure 9. Control of the relative phase of $d[n]$ - σ-constraint.

is compared to the widely known leaky-LMS one. Amplitude and relative-phase of a pure-sinusoid disturbance have been controlled at one of two targeted positions inside a simplified car cavity, which was modelled by using a coupled FE/FE vibro-acoustic formulation. As expected, while constrained decentralized controllers attempted to minimize the cost function at the driver's position, keeping low distortion levels at the passenger's position, the unconstrained decentralized controller attained all the desired control goals, at the expense of causing large distortions. Computer simulations show that the proposed algorithm, besides allowing the explicit association of the adaptive filter gains of the whole system to the q^{th} filter gain, almost attains the same results as the obtained ones with the leaky-LMS strategy, regarding reduction of distortion at other channels. However, since the level of gain restriction obtained through examining the second control module was lower than the obtained one by using the leak parameter, the proposed algorithm was shown to perform better regarding attainment of control goals, at the expense of slightly increase the distortion at the second channel, but keeping stability during uptime.

Acknowledgement

This project has been funded by the São Paulo Research Foundation (FAPESP) - Brazil, under grant # 2012/15783-8. The participation of J. A. Mosquera-Sánchez at KU Leuven has also been funded by FAPESP Brazil, under grant # 2014/09894-7. The authors also acknowledge the support of the European Commission ANTARES and EMVeV research projects, as well as the financial support of SOC project.

References

[1] A. P. Berkhoff. Optimum sensor-actuator distance for decentralized acoustic control. *Journal of the Acoustical Society of America*, 110:260 – 266, 2001.

[2] L. P. R. de Oliveira, M. M. da Silva, J. A. Mosquera-Sánchez, and L. A. M. Gonçalves. Loudness scattering due to vibro-acoustic model variability. *J. of the Braz. Soc. of Mech. Sci. & Eng.*, 34(spe2):604 – 611, 2012.

[3] L. P. R. de Oliveira, B. Stallaert, W. Desmet, J. Swevers, and P. Sas. Optimisation strategies for decentralized ASAC. In *Proceedings of the Forum Acousticum 2005*, pages 875 – 880, 2005.

[4] L. P. R. de Oliveira, B. Stallaert, K. Janssens, H. Van Der Auweraer, P. Sas, and W. Desmet. NEX-LMS: A novel adaptive control scheme for harmonic sound quality control. *Mechanical Systems and Signal Processing*, 24:1727 – 1738, 2010.

[5] S. J. Elliott and C. Boucher. Interaction between multiple feedforward active control systems. *IEEE Transactions on Speech and Audio Processing*, 2:521 – 530, 1994.

[6] S. J. Elliott, I. M. Stothers, and P. A. Nelson. A multiple error LMS algorithm and its application to the active control of sound and vibration. *IEEE Transactions on Acoustics, Speech, and Signal Processing*, ASSP-35:1423 – 1434, 1987.

[7] J. A. Mosquera-Sánchez and L. P. R. de Oliveira. A MIMO control strategy for the sound quality of multi-harmonic disturbances transmitted into cavities. In *22nd International Congress of Mechanical Engineering - COBEM*, 2013.

[8] J. A. Mosquera-Sánchez and L. P. R. de Oliveira. A multi-harmonic amplitude and relative-phase controller for active sound quality control. *Mechanical Systems and Signal Processing*, 45(2):542 – 562, 2014.

[9] B. Rafaely and S. J. Elliott. A computationally efficient frequency-domain LMS algorithm with constraints on the adaptive filter. *IEEE Transactions on Signal Processing*, 48:1649 – 1655, 2000.

[10] S. S. Rao. *Engineering Optimization*. John Wiley & Sons, 4th edition, 2009.